Structure–performance descriptors and the role of Lewis acidity in the methanol-to-propylene process

Irina Yarulina[1,2], Kristof De Wispelaere[3], Simon Bailleul[3], Joris Goetze[4], Mike Radersma[1], Edy Abou-Hamad[5], Ina Vollmer[1], Maarten Goesten[6], Brahim Mezari[6], Emiel J. M. Hensen[6], Juan S. Martínez-Espín[7], Magnus Morten[7], Sharon Mitchell[8], Javier Perez-Ramirez[8], Unni Olsbye[7], Bert M. Weckhuysen[4], Veronique Van Speybroeck[3], Freek Kapteijn[1] and Jorge Gascon[1,2]*

The combination of well-defined acid sites, shape-selective properties and outstanding stability places zeolites among the most practically relevant heterogeneous catalysts. The development of structure–performance descriptors for processes that they catalyse has been a matter of intense debate, both in industry and academia, and the direct conversion of methanol to olefins is a prototypical system in which various catalytic functions contribute to the overall performance. Propylene selectivity and resistance to coking are the two most important parameters in developing new methanol-to-olefin catalysts. Here, we present a systematic investigation on the effect of acidity on the performance of the zeolite 'ZSM-5' for the production of propylene. Our results demonstrate that the isolation of Brønsted acid sites is key to the selective formation of propylene. Also, the introduction of Lewis acid sites prevents the formation of coke, hence drastically increasing catalyst lifetime.

The methanol-to-olefins (MTO) process is a prototypical case study of zeolite catalysis with the potential to alleviate the progressively growing demand for olefins[1]. Zeolites containing Brønsted acidity are the catalysts of choice[2], with ZSM-5 and SAPO-34 being the two materials applied industrially[3]. Zeolite topology is an important parameter[4], however, it is not the only one that defines MTO catalyst performance[5]. Accessibility[6], strength, distribution[7], amount[8] and the nature[9] of acid sites are also of high importance.

Brønsted acid sites (BAS) are believed to be the active sites for olefin production[5,10], however there is currently a consensus that the production of olefins proceeds through an autocatalytic reaction. Accordingly, adsorbed hydrocarbon species in the micropores of a zeolitic catalyst, typically alkenes and arenes, act as 'co-catalyst pool species' (Fig. 1a). Both species participate in two competitive reaction pathways, mechanistically described by the dual-cycle concept: reaction products may either be formed through an alkene- or aromatic-based cycle via methylation/cracking reactions, depending on the nature of the hydrocarbon pool (HP) species[5,11,12].

Optimization of the active site has primarily focused on the nature of the BAS and the HP species. Herein, we show that the active site has an even higher degree of complexity: the combined presence of BAS and Lewis acid sites (LAS) may drastically improve the overall performance of the catalyst. Olefin selectivity and resistance to coking are the two most important parameters in developing new catalysts for this process. In the past few decades, modification of ZSM-5 zeolites with different elements like phosphorus, boron or alkaline-earth

metals[13] has been shown to strongly improve the selectivity to propylene and, simultaneously, improve catalyst lifetime. This sets up the grounds for the methanol-to-propylene (MTP) process: carried out over mildly Brønsted acidic ZSM-5 catalysts at slightly higher temperatures than classical MTO chemistry ($T \geq 500\,°C$). The improved propylene yields have been rationalized on the basis of the lower density of BAS and, in some cases, spatial constrains due to post-synthetic modifications[14], however no clear structure–performance descriptors have been developed.

Here we present a systematic investigation on the effect of acid-site isolation and Brønsted and Lewis acidity on the performance of ZSM-5 zeolites in the MTO process. By establishing a correlation between the type and concentration of acid sites with lifetime and selectivity to ethylene and propylene, we decouple the effect of Brønsted acidity from the effect of Lewis acidity, further determining the respective contributions of BAS and LAS. Next, by combining theory with operando UV–vis and ^{1}H NMR we are able to understand the role of Lewis acidity and to demonstrate that these sites are not spectators. Indeed, LAS become an integral part of the active site and influence the reactivity of intermediates in the HP cycle. The established structure–performance relationships may be applied to other high-temperature zeolite-catalysed reactions.

Results

Assessing textural and acidic properties of the catalysts. We prepared three series of ZSM-5 zeolites with different amounts and

[1]Catalysis Engineering, Chemical Engineering Department, Delft University of Technology, Delft, the Netherlands. [2]King Abdullah University of Science and Technology, KAUST Catalysis Center, Advanced Catalytic Materials, Thuwal, Saudi Arabia. [3]Center for Molecular Modeling, Ghent University, Zwijnaarde, Belgium. [4]Inorganic Chemistry and Catalysis, Debye Institute for Nanomaterials Science, Utrecht University, Utrecht, the Netherlands. [5]King Abdullah University of Science and Technology (KAUST), Core Labs, Thuwal, Saudi Arabia. [6]Schuit Institute of Catalysis, Laboratory of Inorganic Materials Chemistry, Eindhoven University of Technology, Eindhoven, the Netherlands. [7]Centre for Materials Science and Nanotechnology, Department of Chemistry, University of Oslo, Oslo, Norway. [8]Institute for Chemical and Bioengineering, Department of Chemistry and Applied Biosciences, ETH Zurich, Zurich, Switzerland. *e-mail: jorge.gascon@kaust.edu.sa
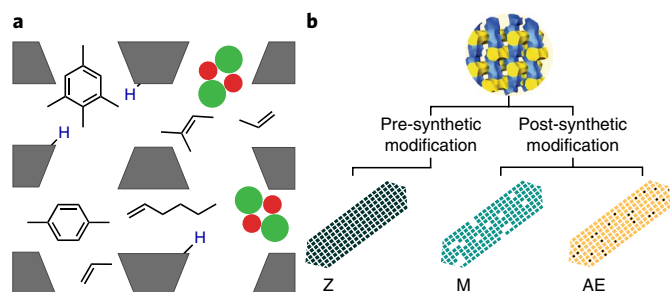
Fig. 1 | Schematic illustrations of the HP concept for the MTO reaction and the synthesis of pre- and post-synthetically modified zeolites.
a, Representation of a ZSM-5 catalyst with Brønsted acid sites (blue) located at the intersection of straight and sinusoidal channels and Lewis acid sites appearing due to the incorporation of extraframework species (green and red). During MTO reaction, ZSM-5 channels are 'inhabited' by olefins and aromatics, which act as 'co-catalysts pool species'.
b, Series Z was prepared by varying the Si/Al ratio and/or SDA during the ZSM-5 zeolite synthesis, series M was prepared by post-synthetic demetallation of microporous ZSM-5 zeolite, whereas series AE was prepared by post-synthetic incorporation of alkaline-earth metals into microporous ZSM-5 zeolite.

types of acid sites. We followed two main approaches: (i) controlling the amount of acid sites and their location during zeolite synthesis, and (ii) modifying the acidity of pre-synthesized zeolites (Fig. 1b). The first series of pre-synthetically modified zeolites (**Z**) was prepared by varying the amount of Al in the synthesis gel and/or utilizing different structure-directing agents (SDA). Another two series of catalysts were obtained following different protocols of post-synthetic modification using commercial Z1 as the starting material. The **M**-series was obtained by Z1 demetallation with various desilicating and dealuminating agents, whereas the **AE**-series was prepared by incorporation of different amounts and types of alkaline-earth metal (AE1–AE5 are Ca-modified, AE6 is Sr-modified and AE7 is Mg-modified).

All synthesized zeolites from the Z-series have the expected MFI topology, comparable morphology and crystal size (Supplementary Figs. 1, 2). Variation of Al during the synthesis resulted in zeolites with different Si/Al ratios (260 and 1,280 for Z2 and Z3, respectively), whereas variation in SDA affected textural properties. N_2 adsorption reveals the existence of a hysteresis loop in the pre-capillary condensation region of microporous Z2 and Z3 (Supplementary Figs. 3, 4) attributed to the phase transition from a disordered phase to a lattice-like fluid phase[15]. This becomes less evident with increasing Al content and completely disappears for Z1 with Si/Al = 40. Z4, synthesized using a di-quaternary ammonium-type surfactant as described previously[16], additionally exhibits a hysteresis loop at high relative pressures, indicative of mesoporosity between stacked sheets[17].

FT-IR spectroscopy of pyridine adsorbed (Supplementary Fig. 5) indicates a decrease in Brønsted acidity[18] (absorbance at 1,546 cm^{-1}) in the Z1–Z4 series, in line with the increasing Si/Al ratio. For the M-series, treatment with various demetallating agents caused a decrease of BAS in comparison to Z1 (Table 1) and resulted in an increased amount of LAS. Lewis acidity is due to the presence of extraframework Al and/or perturbed Al species[19]. Another side-effect of this post-synthetic modification was the generation of mesopores, which are generally held responsible for lifetime improvement in methanol conversion[20,21]. For all samples except M4, demetallation caused a significant increase in the mesoporous surface area (Table 1). Contrastingly, incorporation of alkaline-earth metals resulted in a significant decrease of both

surface area (S_{BET}) and pore-volume (V_p), both gradually reduced with an increase of alkaline-earth loading (Supplementary Fig. 3). Besides, the modification also caused almost a tenfold decrease in BAS concentration (from 232 μmol g^{-1} to 27 μmol g^{-1} for Z1 and AE4). Another clear difference between the Z1 sample and the AE series is the appearance of a significantly higher concentration of LAS (Supplementary Fig. 5).

Comparison of the acidic properties of the studied catalysts reveals that Z3 possesses the same concentration of BAS as AE4 and AE5. The only difference between these samples is the presence of a notable amount of LAS resulting from Ca incorporation. To gain insight into the proximity between these two acid functionalities, two-dimensional ^{1}H–^{1}H DQ (double-quantum) and ^{1}H–^{1}H RFDR (radio-frequency-driven recoupling) MAS NMR was carried out (Fig. 2). These two methods are particularly powerful when combined: RFDR gives a self-correlation peak, whereas DQ does not[22]. The cross-peaks in the horizontal frequency span of 1–2 ppm belong to both terminal Si-OH protons and bridging Ca-OH protons (Fig. 2)[22,23]. When AE3 is fully dehydrated at 450 °C (Supplementary Fig. 6), the DQ correlation vanishes, but the RFDR correlation does not. This indicates that, under reaction conditions, the acidic protons behave as isolated entities.

Effect of pre-synthetic and post-synthetic modification. The impact of acidic properties was evaluated under conditions relevant for the MTO process. Z1 exhibits the shortest lifetime in comparison to the other samples, it deactivates after 16.5 h on stream, which corresponds to an integral throughput of 132 g$_{MeOH}$ g$_{catalyst}$$^{-1}$ (Fig. 3a,b). The lower concentration of Brønsted acidity in Z3 extends the catalyst lifetime up to 28 h (Fig. 3b, Supplementary Fig. 7)[24]. According to a previous study[24], the lower the Si/Al, the faster the formation rate of methylated aromatic species, in turn leading to faster coking rates. Z3 is characterized by steady formation of all products, propylene being the dominant one (up to 48%) (Supplementary Fig. 7). Another striking difference is the much lower fraction of paraffins, ethylene and aromatics in comparison with Z1 (Supplementary Fig. 10). It has been previously demonstrated[11] that the formation of ethylene is mechanistically separated from other olefins, being mostly formed via xylenes and/or trimethylbenzenes, whereas propylene is selectively formed via methylation and cracking reactions within the alkene cycle (Fig. 4b). The formation of paraffins is a result of hydrogen transfer to olefins, where methanol can act as hydrogen donor. Proton transfer occurs on both BAS[25] and extraframework aluminium species[26]. The sharp decrease in formation of ethylene and aromatics in sample Z3 suggests almost full suppression of the aromatic cycle[3,20,26]. As hypothesized previously[27], the aromatic cycle dominates when zeolites with high acid site densities are used. In this line, isolation of BAS by decreasing the Al content leads to higher propylene yields[1]. Further comparison of Z3 with AE5 confirms that the concentration of BAS is indeed the main descriptor for the observed selectivity (Supplementary Fig. 8). These two catalysts, having very similar concentrations of acid sites, exhibit almost identical selectivity to paraffins, ethylene and propylene. In contrast, AE5, prepared by post-synthetic modification with Ca, displays a two times longer lifetime (Fig. 3b). The only obvious difference between these two catalysts is the presence of Lewis acidity in AE5 arising from Ca incorporation.

Demetallated mesoporous M1–M4 show longer lifetimes and higher selectivities to propylene in comparison with the parent Z1 (Supplementary Fig. 9). The improved stability towards deactivation of mesoporous zeolites is generally explained by a facilitated molecular transport[28], along with a higher external surface area that provides more space for coke deposition[29,30]. On the other hand an increased selectivity to propylene can be explained by the decreased concentration of acid sites, the latter being also responsible for the

Table 1 | Textural and acidic properties of the ZSM-5 zeolites under study.

Catalyst	Si/Al[a] (mol mol^{-1})	Cation[b] (%)	V_{total}[c] (cm^3 g^{-1})	V_{micro}[c] (cm^3 g^{-1})	S_{BET}[d] (m^2 g^{-1})	S_{meso}[b] (m^2 g^{-1})	S_{micro}[e] (m^2 g^{-1})	n_{BAS}[f] (µmol g^{-1})	n_{LAS}[f] (µmol g^{-1})
Z1	39	–	0.26	0.15	448	85	363	232	35
Z2	260	–	0.22	0.15	425	85	340	50	12
Z3	1,280	–	0.21	0.17	429	74	355	28	11
Z4	61	–	0.67	0.09	535	328	207	96	74
M1	65	–	1.20	0.12	575	314	261	149	77
M2	36	–	0.35	0.14	456	142	314	188	53
M3	31	–	0.43	0.14	584	276	308	154	108
M4	41	–	0.28	0.11	347	127	220	49	50
AE1	42	Ca (6.1)	0.21	0.11	323	56	267	128	1
AE2	45	Ca (0.2)	0.27	0.15	429	85	344	138	108
AE3	47	Ca (2.4)	0.24	0.13	392	77	315	40	228
AE4	46	Ca (3.8)	0.22	0.13	387	74	313	27	240
AE5	46	Ca (4.6)	0.23	0.12	385	75	310	29	240
AE6	45	Sr (5.2)	0.20	0.13	379	106	273	85	108
AE7	44	Mg (1.4)	0.22	0.14	417	95	322	76	217

[a]Molar ratio determined by ICP-OES. [b]AE1 was prepared by solid-state ion-exchange with Ca(CH$_3$COO)$_2$. AE2 was prepared by ion-exchange with 1 M Ca(NO$_3$)$_2$·4H$_2$O. AE3–AE5 were prepared by incipient wetness impregnation with aqueous solutions of Ca(NO$_3$)$_2$·4H$_2$O of different concentrations. AE6 and AE7 were prepared by incipient wetness impregnation with Sr(NO$_3$)$_2$ and Mg(NO$_3$)$_2$·6H$_2$O, respectively. Further details are provided in the Methods section. [c]From N$_2$ adsorption isotherm using the t-plot method. [d]From N$_2$ adsorption isotherm using the BET method. [e]From N$_2$ adsorption isotherm. $S_{micro} = S_{BET} - S_{meso}$. [f]Concentrations of BAS and LAS derived from FT-IR spectroscopy with pyridine as a probe molecule.
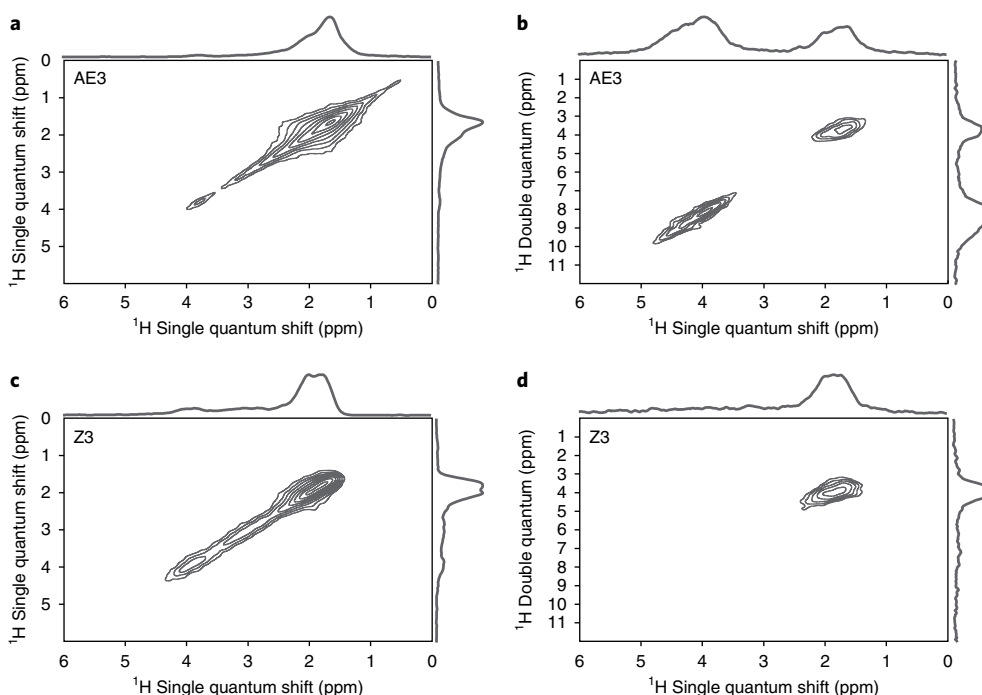

Fig. 2 | Evaluation of Brønsted and Lewis acid site interactions. a–d, ^{1}H–^{1}H RFDR (**a,c**) and ^{1}H–^{1}H DQ (**b,d**) MAS NMR spectra of AE3 modified with Ca (**a,b**) and Z3 with the same amount of BAS (**c,d**). Both samples were dehydrated at 200 °C (1 °C min^{-1}).

improved lifetimes[20,30]. Further examination of the textural and catalytic properties reveals a linear correlation between mesopore surface area and catalyst lifetime (Supplementary Fig. 11). Analysis of the spent catalyst indicates a significantly higher amount of coke deposited in micro- and mesopores for the M-series of zeolites in comparison with Z1. Another striking observation is the significantly longer lifetime of M4, having the lowest surface area in comparison with other samples from the M-series. In the same manner,

Z2 and M4 are rather similar both in porosity and concentration of BAS, but differ in concentration of LAS.

Establishing acidity–performance relationship. The integral propylene selectivity was related to changes in BAS concentration. To account for changes in textural properties, we normalized the concentration of BAS (n_{BAS}) by the BET area (S_{BET}) to yield an acid site surface density (c_{BAS}). During the normalization procedure, we
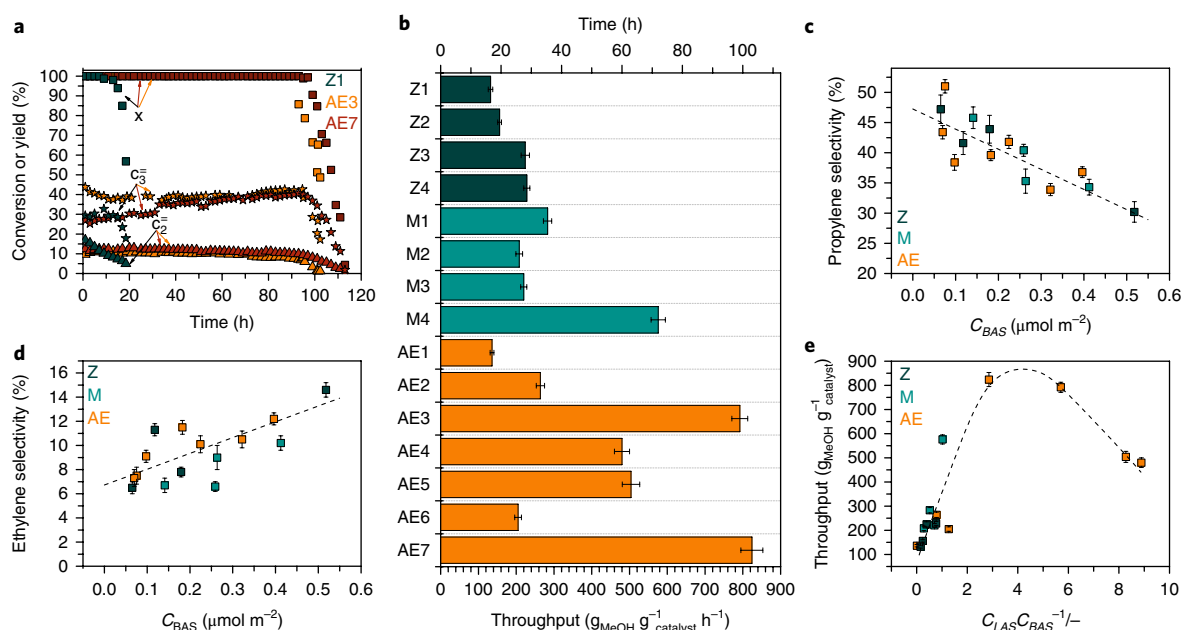
Fig. 3 | Catalytic behaviour of pre- and post-synthetically modified catalysts. a, The modification with Ca (AE3) and Mg (AE7) leads to significant prolongation of catalyst lifetime (black squares), increases yield of propylene (black stars) and decreases yield of ethylene (black triangles). **b**, Methanol throughput and lifetimes of catalysts under study. Reaction conditions: $T = 500\,°C$, WHSV = 8 $g_{MeOH}\,g_{catalyst}^{-1}\,h^{-1}$. **c–e**, Descriptors of ZSM-5 acidity in MTO. Z (black), pre-synthetically modified ZSM-5 with different Si/Al ratio; M (green), post-synthetically demetallated ZSM-5; AE (orange), zeolites modified by post-synthetic incorporation of alkaline-earth metals. The acidity–performance relationship clearly shows that the density of BAS (C_{BAS}) determines propylene (**c**) and ethylene (**d**) selectivity, whereas the ratio of LAS and BAS (C_{BAS}/C_{LAS}) governs catalyst lifetime (**e**). Error bars represent standard deviation of the catalytic performance results performed at least two times for each sample. Dashed lines in **c** and **d** represent linear fit to the provided data, whereas the dashed line in **e** is to guide the eye.

assumed an even distribution of Al within the zeolite framework. This assumption was later validated by UV–vis spectroscopy (vide infra) and ^{27}Al NMR experiments (Supplementary Figs. 12–14).

Figure 3c,d shows the integral propylene and ethylene selectivity as a function of BAS density. These figures clearly demonstrate a linear correlation between C_{BAS} and selectivity to propylene and ethylene for all samples. At high BAS densities, acid sites are in closer proximity. As a consequence, successive reactions can occur at these sites along the diffusion pathway, promoting the aromatic cycle[27]. Low BAS densities prevent consecutive reactions leading to aromatization and coking, thus favouring methylation and cracking reactions. Altogether, these results confirm that BAS isolation is instrumental to attain a high propylene selectivity. Opposite trends obtained for ethylene and propylene also confirm that these two products are formed through two competitive routes. To decrease the impact of the 'secondary reactions' we also plotted ethylene and propylene selectivity taken at 98% oxygenate conversion (Supplementary Fig. 15), that is, when almost the entire catalytic bed is deactivated and only the lower part participates in MTO. As it can be observed, similar correlations are obtained.

The relationship between C_{BAS} and methanol throughput is more complex. Although high BAS densities result in faster deactivation due to faster coking rates, not only BAS density but also distribution play an important role. It has been shown previously[7] that the same concentration of BAS can still lead to different lifetimes due to an uneven Al distribution and formation of Al pairs. Analysis of Al distribution by UV–vis of Co-exchanged zeolites shows that this distribution within $α$-, $β$- and $γ$-sites is rather similar (Supplementary Fig. 12), excluding the effect of Al location. Therefore, the different resistance to deactivation of AE5 and Z3 with similar C_{BAS} is a strong argument to claim that C_{BAS} is not the only descriptor for catalyst lifetime. The same discussion holds for Z2 and M4, the

latter being stable for at least three times longer. Considering that demetallation of M4 did not result in significant development of the external surface area, the potential effect of mesopores on catalyst lifetime can be ruled out. Preparation of M4 involved extraction of framework Al by steaming, leading to the formation of 'inefficient' occluded mesopores barely impacting intracrystalline diffusion[31–33]. It has been shown[6] that interconnectivity of mesopores in hierarchical ZSM-5 has the largest impact on lifetime. This catalyst however showed the longest lifetime among the M-series. As the only obvious difference between these catalysts (AE5 versus Z3 and M4 versus Z3) is the presence of LAS, it seems logical to study the effect of C_{LAS}. Figure 3e shows the methanol throughput plotted as a ratio of LAS and BAS. The obtained 'volcano' plot yields an optimum LAS/BAS ratio between 2 and 6. Interestingly, the two optimal catalysts are AE3 and AE7, samples prepared by Ca and Mg incorporation, respectively, both with an AE/Al molar ratio of 1.8.

On the role of Lewis acidity. The impact of Lewis acidity on MTO is not yet fully understood. There are only a few works dealing with this topic and often reporting a rather negative influence on performance[26]. The majority of those works focus on the presence of extraframework Al (EFAl). Here, we investigate the beneficial effect of alkaline-earth metal modification at the molecular level by performing a series of density functional theory (DFT) based simulations. Earlier, we proposed [Ca(μ-O)(μ-OH)Ca]+ moieties as possible active sites in the Ca-modified ZSM-5 catalyst[34], inspired by the experimentally defined optimal Ca:Al ratio of 2 and the literature reports that divalent extraframework cations tend to self-organize into binuclear complexes in zeolites[35]. We studied the stability of various Ca binuclear complexes when incorporated in a ZSM-5 structure containing two BAS per unit cell. The [Ca(μ-O)$_2$Ca] has a very high basicity and quickly deprotonates the vicinal BAS.
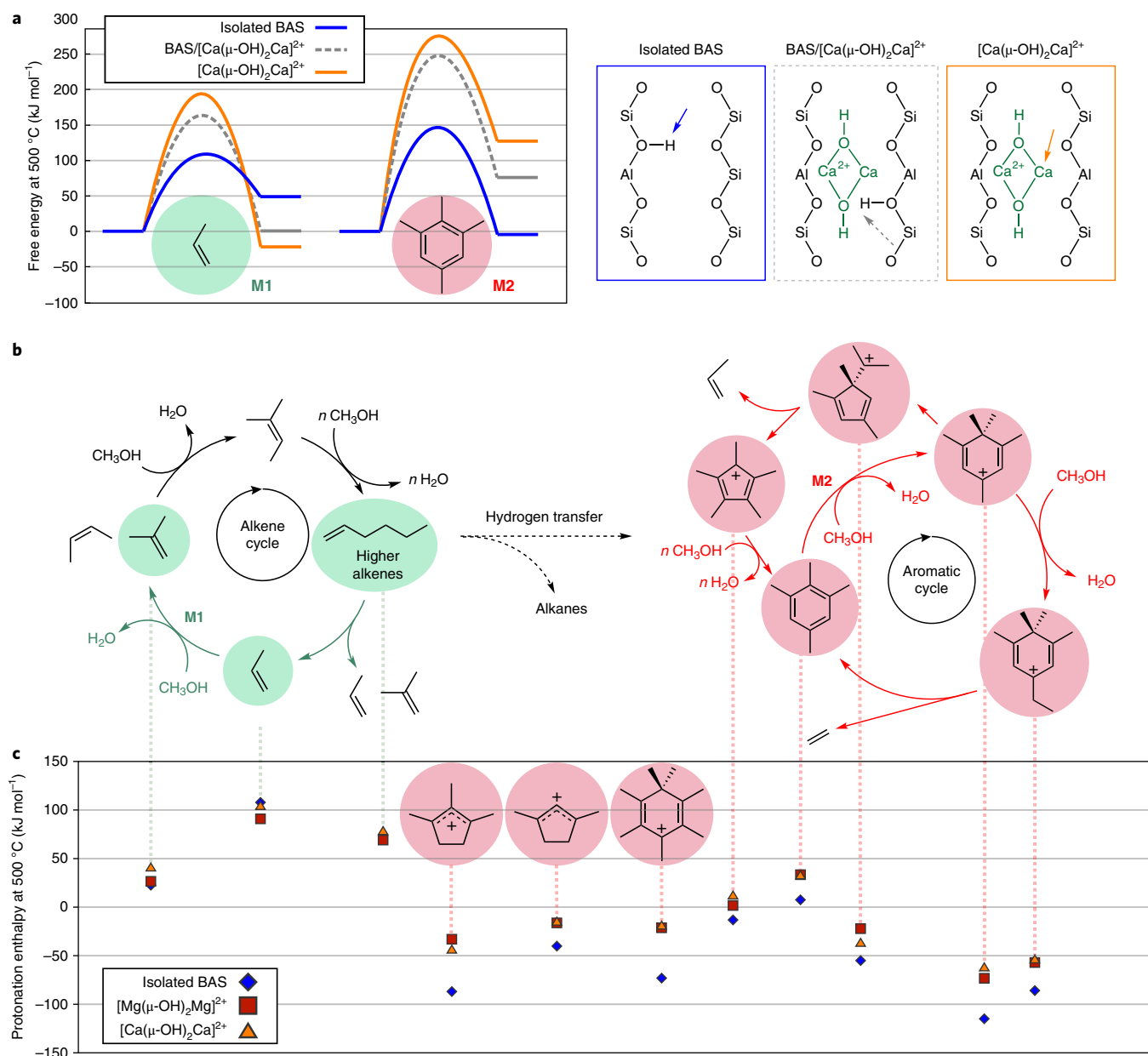
Fig. 4 | Modified zeolites decrease the stability and growth rate of aromatic MTO intermediates. a, Free energy profiles at 500 °C (kJ mol^{-1}) for propene and 1,2,3,5-tetramethylbenzene methylation by methanol catalysed by an isolated BAS, a BAS near a $[Ca(\mu-OH)_2Ca]^{2+}$ moiety and an LAS formed by the $[Ca(\mu-OH)_2Ca]^{2+}$ site. **b,** The dual cycle mechanism for the MTO process with indication of intermediates that are unaffected by the alkaline-earth modification (green) and destabilized by the modification (red). **c,** Calculated protonation enthalpies at 500 °C (kJ mol^{-1}) for the various MTO intermediates at an isolated BAS (blue diamonds) in the presence of a $[Mg(\mu-OH)_2Mg]^{2+}$ (red squares) or a $[Ca(\mu-OH)_2Ca]^{2+}$ (orange triangles) moiety.

An alternative stabilizing interaction for the singly protonated $[Ca(\mu-O)(\mu-OH)Ca]^+$ is to bind to the zeolite framework, but this is by far less stabilizing than the formation of $[Ca(\mu-OH)_2Ca]^{2+}$ (Fig. 5). This analysis clearly shows the capacity of alkaline earth modification to reduce the number of BAS sites in the catalyst.

Further, we investigated the reactivity and stability of some key HP species at LAS and BAS. Figure 4a shows that the free energies of activation for the methylation reactions of propene and 1,2,3,5-tetramethylbenzene (tetraMB) significantly increase upon Ca incorporation. The obtained transition states are shown in Supplementary Figs. 26 and 27. These two reactions are crucial for the alkene and aromatics catalytic cycles[36–38]. When the reaction is catalysed by a BAS near a Ca moiety (BAS/$[Ca(\mu-OH)_2Ca]^{2+}$) or by a LAS formed by the $[Ca(\mu-OH)_2Ca]^{2+}$ moiety, the free energy barriers increase

by 54–67 kJ mol^{-1} for propene and 101–129 kJ mol^{-1} for tetraMB compared to the reactions catalysed by an isolated BAS. Thus, alkene and aromatics methylation are slowed down to a different extent in Ca-ZSM-5. These results show that the growth of aromatics by methylation, and thus the propagation of the aromatics-based HP cycle, is strongly suppressed by Ca incorporation while alkene methylation and the propagation of the autocatalytic cycle can still take place. These calculations were experimentally verified by co-feeding benzene with DME over samples Z3 and AE5. The apparent activation energy of benzene methylation increased from 64 kJ mol^{-1} over Z3 to 85 kJ mol^{-1} over AE5 (Supplementary Fig. 21). In line with this observation, higher selectivity to secondary products was observed over Z3 than over AE5 (Supplementary Fig. 20). At 500 °C, alkaline earth modification was found to decrease the
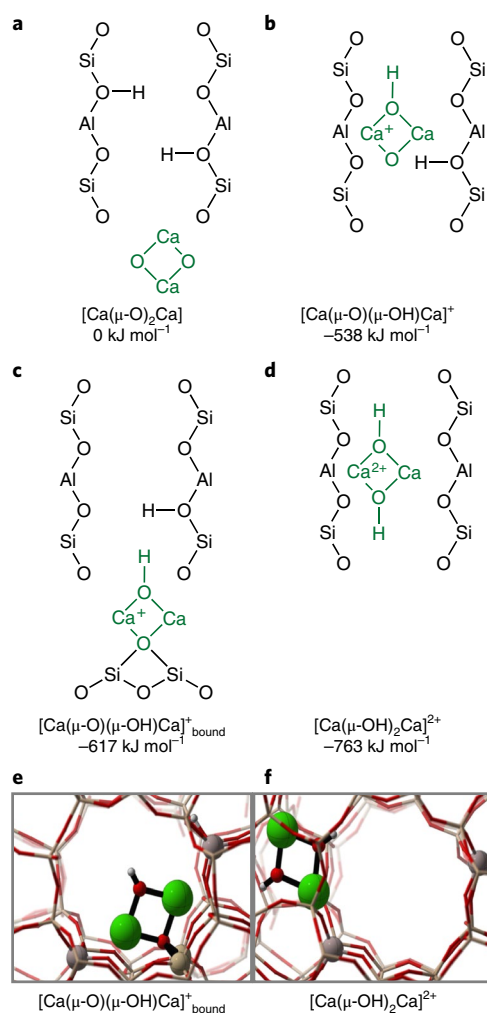
Fig. 5 | DFT-based enthalpy calculations at 500 °C reveal the most stable structure of binuclear Ca species in ZSM-5. a–f, Reference state (**a**), [Ca(μ-O)(μ-OH)Ca]$^+$ compound in ZSM-5 (**b**), [Ca(μ-O)(μ-OH)Ca] bound to the framework (**c**), [Ca(μ-OH)$_2$Ca]$^{2+}$ in ZSM-5 (**d**), snapshot of [Ca(μ-O)(μ-OH)Ca] bound to the framework (**e**) and snapshot of [Ca(μ-OH)$_2$Ca]$^{2+}$ in ZSM-5 (**f**).

rate of benzene conversion by a factor of 4.1. Similar co-feeding experiments with isobutene also indicate a decrease of the rate of isobutene conversion by a factor of 2.4 at 500 °C, which is smaller than for benzene conversion. We further investigated the stability of carbocations, which are known to be key intermediates in the aromatic cycle[39]. Proton enthalpies for a series of MTO intermediates were studied in ZSM-5 samples with an isolated BAS and samples with a BAS nearby a [Ca(μ-OH)$_2$Ca]$^{2+}$ or [Mg(μ-OH)$_2$Mg]$^{2+}$ site. The selection of HP species is inspired by the proposed intermediates in the alkene and aromatic-based cycle[40]. We found that the stability of carbenium ions is largely reduced in LAS-modified zeolites, for example the protonation enthalpy of 1,2,2,3,5-pentamethylbenzenium ion reduces from −120 kJ mol^{-1} to −75 and −65 in Mg- and Ca-modified zeolites (Fig. 4c). The difference in protonation enthalpies may be ascribed to the stabilizing interaction of the double bonds of the neutral cyclic species with the [Ca(μ-OH)$_2$Ca]$^{2+}$ sites. Our findings show that cyclic HP intermediates formed in LAS-modified zeolites would be much less reactive in the aromatic based cycles. The influence on alkenes is far less pronounced, which is an indication that this cycle is less affected by incorporating LAS. These conclusions are fully in line

with the free energy profiles for methylation of propene and tetraMB shown in Fig. 4a. We also investigated the lifetimes of neutral species at a realistic working condition of 500 °C (Supplementary Fig. 41). We performed molecular dynamics simulations on the neutral species and investigated the tendency of the zeolite framework to protonate the HP compounds. In accordance with our static simulations, systematically longer lifetimes are found for the neutral species in LAS -modified zeolites. We observe similar features for EFAl species with a [HOAl(μ-OH)$_2$AlOH]$^{2+}$ structure, indicating similarities between EFAls and Ca species (see Supplementary Figs. 34–38).

Operando UV–vis diffuse reflectance spectroscopy (UV–vis DRS) is an insightful technique to follow the evolution of HP formed in a zeolitic microenviroment[41–43], able to distinguish between different neutral and protonated species. To identify experimentally whether the presence of Lewis acidity affects the nature of HP species, we monitored the formation of hydrocarbons produced during MTO via UV–vis DRS for Ca-containing AE3 and compared the obtained spectra with Z1 and Z2. The spectra of Z1 and Z2 taken during the first minutes of MTO are characterized by similar absorption bands but different intensities (Fig. 6 and Supplementary Fig. 16). This points to the fact that hydrocarbon species are of the same nature but form in different amounts, the nature of hydrocarbon species is independent from the amount of BAS. In UV–vis, the region above 35,000 cm^{-1} corresponds to neutral aromatic species, while protonated aromatics and neutral polyaromatics absorb light at lower wavenumbers. For samples Z1 and Z2, the first minutes of MTO are characterized by the appearance of a band around 35,000 cm^{-1} corresponding to neutral benzene and a broad component composed by a combination of bands around 23,600, 20,600 and 17,000 cm^{-1} (Supplementary Fig. 16), corresponding to methyl-substituted benzenium cations[41,42]. With time-on-stream, the appearance of the absorption band below 15,000 cm^{-1} (Supplementary Fig. 16) indicates an accumulation of polyaromatic species in Z1 and Z2. The early appearance of this band indicates that formation of polyaromatics starts at the beginning of the reaction (Supplementary Fig. 16). In sharp contrast, the UV–vis DRS of AE3 reveal neither neutral nor charged aromatic species. The spectra are characterized by a wide band around 30,000 cm^{-1} becoming much broader with increasing time-on-stream. Attribution of this region is rather controversial in literature but it is generally agreed that these bands are indicative for monoenylic and dienylic cations[44]. After 5 h on stream, the absorption bands below 15,000 cm^{-1} display the highest intensity for samples Z1 and Z2 pointing at the prevalence of naphthalene and its homologues; they are still not observable for AE3. These observations support the theoretical calculations (vide supra) and suggest that indeed LAS prevent further reactions involving aromatic moieties.

Finally, ^{1}H and ^{1}H–^{1}H DQ MAS NMR experiments at very high spinning speed were performed to validate the nature of trapped species in fully deactivated AE5, Z1 and Z3. The ^{1}H (MAS) NMR spectra of the analysed samples clearly show a difference, especially for the resonance at 7 ppm (Fig. 6b). The signals at 7.8 and 7.1 ppm with a strong autocorrelation in DQ experiments (Fig. 6c,d) are assigned to aromatic hydrogen. In line with UV–vis, MAS NMR also demonstrates that aromatic species do not accumulate in Ca-containing zeolites and play a minor role in catalyst deactivation. The trapped species in Ca-containing AE5 are mainly of aliphatic nature, as confirmed by the resonances appearing in the range between 4.3–0 ppm (ref.[45]).

Discussion
In pursuit of a long-living MTP catalyst, a great number of zeolite-based catalysts with ZSM-5 topology have been engineered[13]. Herein, we identified the main descriptors governing selectivity and lifetime by rationalizing catalytic results of samples prepared
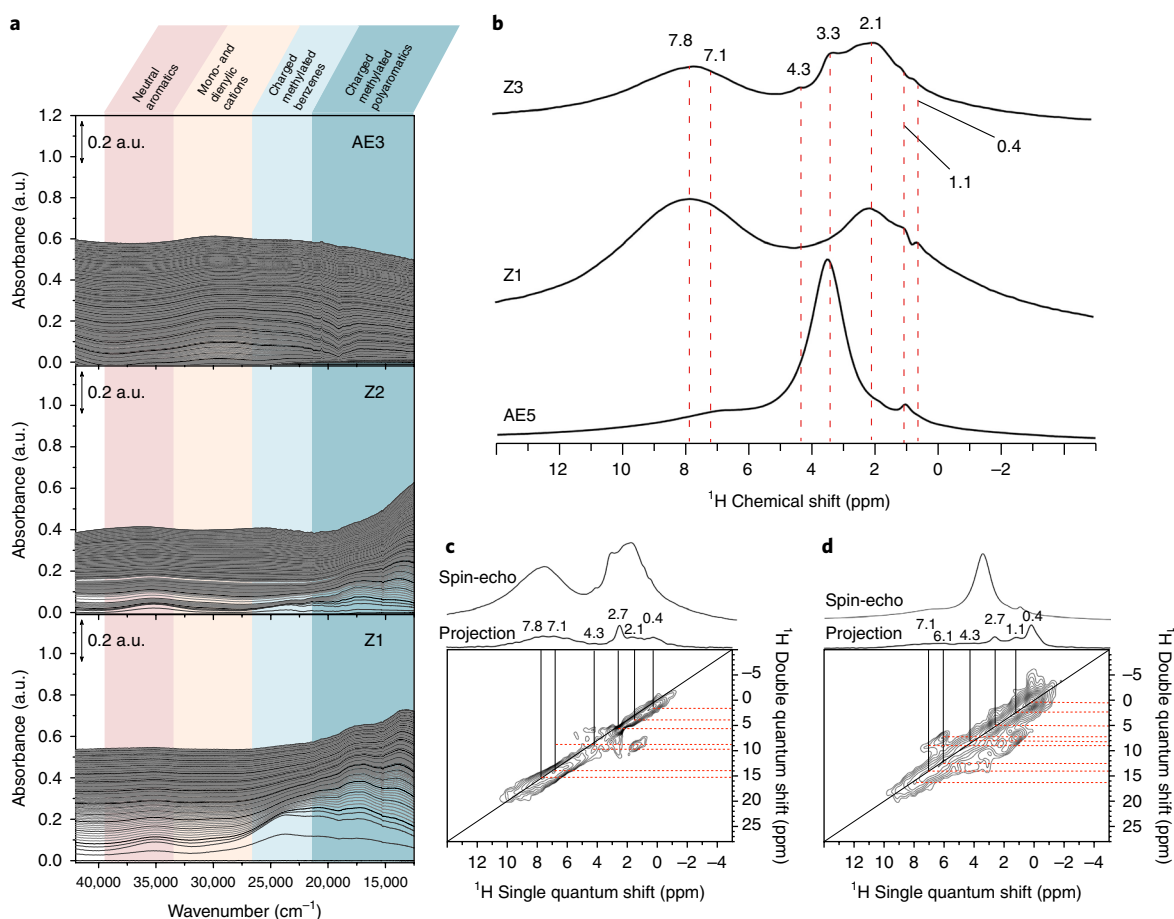
Fig. 6 | Visualization of the trapped hydrocarbon species in Z- and AE-series. a, Operando UV–vis diffuse reflectance spectra collected during methanol conversion over Z1 and Z2 zeolites with different Si/Al ratios and Ca-modified AE3 at 500 °C indicates that aromatic species do not accumulate in Ca-modified samples. For Z1 and Z2 zeolites, formation of polyaromatic species (naphthalene and homologues) is observed during the first seconds of MTO, indicating that catalyst deactivation starts at the beginning of the reaction. UV–vis diffuse reflectance spectra were taken every 20 s. **b**, Analysis of the spent catalyst by ^{1}H NMR indicates further that aromatic species are the minor components in completely deactivated Ca-modified catalysts, which is characterized by the predominant presence of aliphatic protons. **c**, ^{1}H–^{1}H DQ MAS NMR spectra of Z3 shows that aliphatic protons are correlating with aromatic protons, suggesting that trapped species are mainly represented by alkylated aromatics. **d**, In AE5, aliphatic protons are mainly autocorrelated. Black lines indicate peaks in single quantum space, whereas red dashed lines show the (auto-)correlation in DQ space.

by different synthetic protocols. Normalization of acidity by surface area helped elucidate catalytic behaviour not only of microporous but also of mesoporous zeolites, which are generally more stable towards deactivation due to the combination of improved mass-transfer properties and ability to hold more coke. We have demonstrated that BAS isolation and Lewis acidity are the most important parameters in defining catalyst selectivity and lifetime.

We have confirmed that propylene selectivity is controlled by BAS density (C_{BAS}). Acid site isolation is the key to maximize propylene selectivity by preventing secondary reactions leading to the formation of aromatics. Thus, BAS is the first descriptor of catalytic performance, and its influence on product distribution is generally confirmed in the literature[1]. BAS isolation may be achieved using various approaches. Herein, we showed that, apart from decreasing Al content, incorporation of alkaline-earth metals also results in generation of isolated BAS. Taking Ca species as an example, we showed that alkaline-earth metals tend to deprotonate BAS thus neutralizing inherent zeolite acidity, forming $[Ca(\mu\text{-}OH)_2Ca]^{2+}$ species of Lewis acidic nature and isolated BAS, as demonstrated by ^{1}H–^{1}H DQ and ^{1}H–^{1}H RFDR MAS NMR. The generation of a new type of LAS turned out to be critical to obtain long-living catalysts. Catalyst lifetime may be optimized by tuning the

LAS/BAS ratio according to a typical volcano plot. We found that $[Ca(\mu\text{-}OH)_2Ca]^{2+}$ LAS species have the tendency to suppress aromatics growth by methylation and destabilize crucial carbenium ions for the aromatic cycle, thereby blocking this reaction pathway. Hand in glove, UV–vis DRS showed that 'LAS-containing' catalysts do not form polyaromatic species—notorious for catalyst deactivation—in contrast to 'LAS-free' catalysts. For the latter, the formation and evolution of aromatic species was witnessed during the first minutes of MTO independently on the amount of BAS. Finally, the destabilizing effect of LAS presence on aromatic cycle was confirmed by ^{1}H MAS NMR performed on fully deactivated catalysts. The trapped hydrocarbons in the case of Ca-containing samples were mainly aliphatic of nature, while non-modified catalyst materials had a large amount of aromatic species.

With this information in hand, we can now formulate clear design rules to achieve ideal MTO catalysts maximizing propylene selectivity and lifetime. The presented case shows that a subtle interplay between various functions in the catalyst—in this case incorporation of LAS and BAS sites—may be used to obtain an optimally performing catalyst. Given the fact that zeolite catalysis often encounters similar reaction intermediates, we expect that the trends discovered here will also be of high relevance for many other zeolite

catalysed processes, such as catalytic cracking or isomerization. We conceptually showed the potential for tuning active sites in zeolite acid-catalysed reactions to a greater degree of complexity.

Methods

Synthesis of the Z-series catalysts. **Z1** is commercially available ZSM-5 zeolite calcined at 550 °C (CBV 8014, Zeolyst International). **Z2** and **Z3** were hydrothermally synthesized following the procedure described previously[46]. **Z4** was synthesized according to a previous protocol[47]. As-synthesized **Z2**, **Z3** and **Z4** were calcined in air at 550 °C to remove the template, and ion-exchanged with NH_4NO_3 (1 M, 80 °C, 2 h) followed by calcination in air at 500 °C for 5 h.

Synthesis of the M-series catalysts. **M1** was obtained from **Z1** by desilication and acid leaching. Desilication was carried out in 1 M NaOH at 70 °C for 1 h. **M2** and **M3** were obtained by treatment of **Z1** in 0.1 and 0.2 M NaOH at 65 °C for 30 min. In the preparation of **M3**, the treatment solution also contained 0.2 M tetrapropylammonium bromide. Both samples were converted into protonic form by ion exchange in NH_4NO_3 solution (0.1 M, 25 °C, 8 h) and calcined at 550 °C for 5 h. **M4** was obtained from microporous **Z1** by in situ dealumination in two consecutive MTO runs.

Synthesis of the AE-series catalysts. **AE1** was prepared by solid-state ion-exchange with $Ca(CH_3COO)_2$. **AE2** was prepared by triple ion-exchange with 1 M $Ca(NO_3)_2 \cdot 4H_2O$ at 80 °C. **AE3**, **AE4** and **AE5** were prepared by incipient wetness impregnation (IWI) with an aqueous solution of $Ca(NO_3)_2 \cdot 4H_2O$ (2.4 M, 4.0 M and 6.0 M, respectively). **AE6** and **AE7** were prepared by IWI with 2.4 M $Sr(NO_3)_2$ and 2.4 M $Mg(NO_3)_2 \cdot 6H_2O$. After the modification, all AE samples were calcined at 550 °C. Detailed information is further provided in Supplementary Experimental Section.

Characterization. N_2 adsorption at −196 °C was carried out using a Tristar II 3020 analyser (Micromeritics). Microscopy images were recorded using a JEOL JSM-6010LA with a standard beam potential of 10 kV and an Everhart–Thornley detector. The XRD patterns of the powders were recorded with a Bruker D8 Advance X-ray diffractometer equipped with a LynxEye position-sensitive detector and monochromatic CoKα ($\lambda = 1.788970$ Å). Transmission FT-IR spectroscopy using pyridine as a probe molecule was performed using a Nicolet 6700 spectrometer with a MCT/B detector. For the wafer preparation, 50 mg of catalyst was used without any dilution. The amount of Brønsted (BAS) and Lewis (LAS) acid sites was derived from the bands at 1,545 and 1,456 cm^{-1} using extinction coefficients of 1.67 and 2.22, respectively[18]. ^{1}H MAS NMR (magic angle spinning nuclear magnetic resonance) measurements were performed on a 11.7 Tesla Bruker DMX500 NMR spectrometer operating at a ^{1}H Larmor frequency of 500 MHz. A Bruker triple resonance 4 mm MAS probe head with a sample rotation rate of 10 kHz was used. ^{1}H NMR spectra were recorded with a 90° pulse of 5 µs duration and 3 s interscan delay. DQ experiments were performed using the back-to-back (BABA) recoupling sequence for excitation and reconversion of the DQ coherences with a 100 µs duration. The 2D RFDR (radio frequency-driven recoupling) experiments were implemented via the application of rotor-synchronized 180-degree pulses (one inversion pulse per rotor period) for homonuclear dipolar recoupling. A total mixing time duration of 1.6 ms was used. Deactivated zeolite materials were analysed by one-dimensional ^{1}H MAS SS NMR and ^{1}H−^{1}H multiple-quantum spectroscopy. One-dimensional ^{1}H MAS SS NMR spectra were recorded on Bruker AVANCE III spectrometers operating at 600 MHz resonance frequencies for ^{1}H. The sample spinning frequency was 30 kHz for ^{1}H. Two-dimensional DQ experiments were recorded on a Bruker AVANCE III spectrometer operating at 600 MHz with a conventional double-resonance 2.5 mm CP/MAS probe. The ultraviolet–visible diffuse reflectance spectra (UV–vis DRS) were collected on a Perkin–Elmer Lambda 900 spectrophotometer equipped with an integrating sphere (Labsphere) in the 200–800 nm range. The absorption intensity was expressed by the Schuster–Kubelka–Munk equation. Quantification of Al_{pairs} and determination of their location has been reported previously[48]. Operando UV–vis diffuse reflectance spectra were obtained using an AvaSpec 2048L spectrometer connected to a high temperature UV–vis optical fibre probe. The measurements were performed in the wavenumber range 11,000–50,000 cm^{-1}.

Catalyst testing. Catalytic experiments were carried out in a Microactivity Reference unit (PID Eng&Tech) at 500 °C and ambient pressure. The catalyst (pressed, crushed and sieved to particle sizes 250–420 µm) was mixed with SiC (6:1 wt%) and placed in a fixed-bed with an internal diameter of 9 mm for standard experiments. An ISCO pump was used to feed methanol to the reactor system. A weight-hourly space velocity (WHSV) of 8 g$_{MeOH}$ g$_{cat}^{-1}$ h^{-1}, an N_2:MeOH = 1:1 molar feed composition and atmospheric pressure were utilized. Conversion, selectivities and yields were calculated on a molar carbon basis. The performance results are presented in graphs as a function of the methanol mass throughput per amount of catalyst used (g$_{MeOH}$ g$_{cat}^{-1}$) and defined as the overall amount MeOH fed through the catalytic bed before the conversion of oxygenates drops below 80%. Presented

selectivities are integral values. In each case, the catalyst was operated in a fixed bed reactor until methanol conversion dropped below 50%.

Static calculations. Periodic DFT calculations are performed using the Vienna Ab Initio Simulation Package (VASP 5.3) with the PBE functional and using Grimme D3 dispersion corrections[49–52]. During the calculations, the projector augmented wave method is used. Furthermore, a plane-wave cutoff of 600 eV is used during the calculations and the self-consistent field convergence criterion is set to 10^{-5} eV. The sampling of the Brillouin zone is restricted to the Γ-point. The static calculations are performed in a ZSM-5 unit cell consisting of 96 T atoms. More information on the introduction of Al substitutions and unit cell parameters can be found in the Supplementary Computational Section. For a comprehensive overview of the state-of-the-art in modelling zeolite catalysis refer to ref. [38].

Dynamic calculations. The ab initio MD simulations are performed using the CP2K software package[53,54]. To account for the flexibility of the catalyst framework at realistic reaction conditions the NPT ensemble at 673 K and 773 K and 1 bar is used. During the ab initio MD simulations, the temperature is controlled by a chain of five Nosé–Hoover thermostats and the pressure by an MTK barostat. To represent the ZSM-5 zeolite, the same unit cell is used as during the static calculations, so extra information can be found in the Supporting Computational Section.

Code availability. The applied DFT codes (VASP and CP2K) are commercially available. Analysis of static calculations was performed with the TAMkin toolkit, which is freely available from https://molmod.ugent.be/software. Molecular dynamics runs were analysed using the freely available VMD software (http://www.ks.uiuc.edu/Research/vmd/).

Data availability. Data supporting the findings of this study are available within this paper and its Supplementary Information, and are available from the corresponding author upon reasonable request.

References

1. Bleken, F. L. et al. Conversion of methanol into light olefins over ZSM-5 zeolite: strategy to enhance propene selectivity. *Appl. Catal. A* **447**, 178–185 (2012).
2. Keil, F. J. Methanol-to-hydrocarbons: process technology. *Microporous Mesoporous Mater.* **29**, 49–66 (1999).
3. Sun, X. Y. et al. On reaction pathways in the conversion of methanol to hydrocarbons on HZSM-5. *J. Catal.* **317**, 185–197 (2014).
4. Teketel, S. et al. Morphology-induced shape selectivity in zeolite catalysis. *J. Catal.* **327**, 22–32 (2015).
5. Olsbye, U. et al. Conversion of methanol to hydrocarbons: how zeolite cavity and pore size controls product selectivity. *Angew. Chem. Int. Ed.* **51**, 5810–5831 (2012).
6. Milina, M., Mitchell, S., Crivelli, P., Cooke, D., & Perez-Ramirez, J. Mesopore quality determines the lifetime of hierarchically structured zeolite catalysts. *Nat. Commun.* **5**, 3922 (2014).
7. Liang, T. et al. Conversion of methanol to olefins over H-ZSM-5 zeolite: reaction pathway is related to the framework aluminum siting. *ACS Catal.* **6**, 7311–7325 (2016).
8. Yarulina, I. et al. Methanol-to-olefins process over zeolite catalysts with DDR topology: effect of composition and structural defects on catalytic performance. *Catal. Sci. Technol.* **6**, 2663–2678 (2016).
9. Deimund, M. A. et al. Effect of heteroatom concentration in SSZ-13 on the methanol-to-olefins reaction. *ACS Catal.* **6**, 542–550 (2016).
10. Hemelsoet, K., Van der Mynsbrugge, J., De Wispelaere, K., Waroquier, M. & Van Speybroeck, V. Unraveling the reaction mechanisms governing methanol-to-olefins catalysis by theory and experiment. *ChemPhysChem* **14**, 1526–1545 (2013).
11. Svelle, S. et al. Conversion of methanol into hydrocarbons over zeolite H-ZSM-5: ethene formation is mechanistically separated from the formation of higher alkenes. *J. Am. Chem. Soc.* **128**, 14770–14771 (2006).
12. Haw, J. F., Song, W. G., Marcus, D. M. & Nicholas, J. B. The mechanism of methanol to hydrocarbon catalysis. *Acc. Chem. Res.* **36**, 317–326 (2003).
13. Stöcker, M. Methanol-to-hydrocarbons: catalytic materials and their behavior. *Microporous Mesoporous Mater.* **29**, 3–48 (1999).
14. Janardhan, H. L., Shanbhag, G. V. & Halgeri, A. B. Shape-selective catalysis by phosphate modified ZSM-5: Generation of new acid sites with pore narrowing. *Appl. Catal. A* **471**, 12–18 (2014).
15. Llewellyn, P. L. et al. Adsorption by MFI-type zeolites examined by isothermal microcalorimetry and neutron-diffraction. 2. Nitrogen and carbon-monooxide. *Langmuir* **9**, 1852–1856 (1993).

16. Choi, M. et al. Stable single-unit-cell nanosheets of zeolite MFI as active and long-lived catalysts. *Nature* **461**, 246–249 (2009).
17. Cychosz, K. A., Guillet-Nicolas, R., Garcia-Martinez, J. & Thommes, M. Recent advances in the textural characterization of hierarchically structured nanoporous materials. *Chem. Soc. Rev.* **46**, 389–414 (2017).
18. Emeis, C. A. Determination of integrated molar extinction coefficients for infrared-absorption bands of pyridine adsorbed on solid acid catalysts. *J. Catal.* **141**, 347–354 (1993).
19. Brus, J. et al. Structure of framework aluminum Lewis sites and perturbed aluminum atoms in zeolites as determined by Al-27{H-1} REDOR (3Q) MAS NMR spectroscopy and DFT/Molecular mechanics. *Angew. Chem. Int. Ed.* **54**, 541–545 (2015).
20. Mei, C. S. et al. Selective production of propylene from methanol: mesoporosity development in high silica HZSM-5. *J. Catal.* **258**, 243–249 (2008).
21. Milina, M., Mitchell, S., Michels, N. L., Kenvin, J. & Perez-Ramirez, J. Interdependence between porosity, acidity, and catalytic performance in hierarchical ZSM-5 zeolites prepared by post-synthetic modification. *J. Catal.* **308**, 398–407 (2013).
22. Volkringer, C. et al. The Kagome topology of the gallium and indium metal-organic framework types with a MIL-68 tructure: synthesis, XRD, solid-state NMR characterizations, and hydrogen adsorption. *Inorg. Chem.* **47**, 11892–11901 (2008).
23. Ruspic, C. et al. A well-defined hydrocarbon-soluble calcium hydroxide: synthesis, structure, and reactivity. *J. Am. Chem. Soc.* **128**, 15000–15004 (2006).
24. Mores, D., Kornatowski, J., Olsbye, U. & Weckhuysen, B. M. Coke formation during the methanol-to-olefin conversion: in situ microspectroscopy on individual H-ZSM-5 crystals with different Bronsted acidity. *Chem. Eur. J.* **17**, 2874–2884 (2011).
25. Martínez-Espín, J. S. et al. Hydrogen transfer versus methylation: on the genesis of aromatics formation in the methanol-to-hydrocarbons reaction over H-ZSM-5. *ACS Catal.* **7**, 5773–5780 (2017).
26. Müller, S. et al. Hydrogen transfer pathways during zeolite catalyzed methanol conversion to hydrocarbons. *J. Am. Chem. Soc.* **138**, 15994–16003 (2016).
27. Guisnet, M., Costa, L. & Ribeiro, F. R. Prevention of zeolite deactivation by coking. *J. Mol. Catal. A Chem.* **305**, 69–83 (2009).
28. Mitchell, S. et al. Structural analysis of hierarchically organized zeolites. *Nat. Commun.* **6**, 8633 (2015).
29. Schmidt, F. et al. Coke location in microporous and hierarchical ZSM-5 and the impact on the MTH reaction. *J. Catal.* **307**, 238–245 (2013).
30. Bleken, F. L. et al. Catalyst deactivation by coke formation in microporous and desilicated zeolite H-ZSM-5 during the conversion of methanol to hydrocarbons. *J. Catal.* **307**, 62–73 (2013).
31. Kortunov, P. et al. The role of mesopores in intracrystalline transport in USY zeolite: PFG NMR diffusion study on various length scales. *J. Am. Chem. Soc.* **127**, 13055–13059 (2005).
32. Karger, J. & Valiullin, R. Mass transfer in mesoporous materials: the benefit of microscopic diffusion measurement. *Chem. Soc. Rev.* **42**, 4172–4197 (2013).
33. Karger, J. Transport phenomena in nanoporous materials. *ChemPhysChem* **16**, 24–51 (2015).
34. Yarulina, I. et al. Suppression of the aromatic cycle in methanol-to-olefins reaction over ZSM-5 by post-synthetic modification using calcium. *ChemCatChem* **8**, 3057–3063 (2016).
35. Pidko, E. A., Hensen, E. J. M. & van Santen, R. A. Self-organization of extraframework cations in zeolites. *Proc. R. Soc. A* **468**, 2070–2086 (2012).
36. De Wispelaere, K., Bailleul, S. & Van Speybroeck, V. Towards molecular control of elementary reactions in zeolite catalysis by advanced molecular simulations mimicking operating conditions. *Catal. Sci. Technol.* **6**, 2686–2705 (2016).
37. Van Speybroeck, V. et al. First principle kinetic studies of zeolite-catalyzed methylation reactions. *J. Am. Chem. Soc.* **133**, 888–899 (2011).
38. Van Speybroeck, V. et al. Advances in theory and their application within the field of zeolite chemistry. *Chem. Soc. Rev.* **44**, 7044–7111 (2015).
39. Nicholas, J. B. & Haw, J. F. The prediction of persistent carbenium ions in zeolites. *J. Am. Chem. Soc.* **120**, 11804–11805 (1998).
40. Fang, H. et al. Theoretical investigation of the effects of the zeolite framework on the stability of carbenium ions. *J. Phys. Chem. C* **115**, 7429–7439 (2011).
41. Goetze, J. et al. Insights into the activity and deactivation of the methanol-to-olefins process over different small-pore zeolites as studied with operando UV–vis spectroscopy. *ACS Catal.* **7**, 4033–4046 (2017).
42. Hemelsoet, K. et al. Identification of intermediates in zeolite-catalyzed reactions by in situ UV/Vis microspectroscopy and a complementary set of molecular simulations. *Chem. Eur. J.* **19**, 16595–16606 (2013).
43. Goetze, J., Yarulina, I., Gascon, J., Kapteijn, F. & Weckhuysen, B. M. Revealing lattice expansion of small-pore zeolite catalysts during the methanol-to-olefins process using combined operando X-ray diffraction and UV–vis spectroscopy. *ACS Catal.* **8**, 2060–2070 (2018).
44. Wulfers, M. J. & Jentoft, F. C. The role of cyclopentadienium ions in methanol-to-hydrocarbons chemistry. *ACS Catal.* **4**, 3521–3532 (2014).
45. Behera, B., Ray, S. S. & Singh, I. D. NMR Studies of FCC feeds, catalysts and coke. *Fluid Catal. Crack. VII Mater. Methods Process Innov.* **166**, 163–200 (2007).
46. Hong, Y. et al. Platinum nanoparticles supported on Ca(Mg)-zeolites for efficient room-temperature alcohol oxidation under aqueous conditions. *Chem. Commun.* **50**, 9679–9682 (2014).
47. Na, K. et al. Pillared MFI zeolite nanosheets of a single-unit-cell thickness. *J. Am. Chem. Soc.* **132**, 4169–4177 (2010).
48. Dedecek, J., Balgová, V., Pashkova, V., Klein, P. & Wichterlová, B. Synthesis of ZSM-5 zeolites with defined distribution of Al atoms in the framework and multinuclear MAS NMR analysis of the control of Al distribution. *Chem. Mater.* **24**, 3231–3239 (2012).
49. Kresse, G. & Hafner, J. Ab initio. *Phys. Rev. B* **47**, 558–561 (1993).
50. Kresse, G. & Hafner, J. Ab initio. *Phys. Rev. B* **49**, 14251–14269 (1994).
51. Kresse, G. & Furthmüller, J. Efficient iterative schemes for ab initio total-energy calculations using a plane-wave basis set. *Phys. Rev. B* **54**, 11169–11186 (1996).
52. Kresse, G. & Furthmüller, J. Efficiency of ab-initio total energy calculations for metals and semiconductors using a plane-wave basis set. *Comput. Mater. Sci.* **6**, 15–50 (1996).
53. Hutter, J., Iannuzzi, M., Schiffmann, F. & VandeVondele, J. CP2K: atomistic simulations of condensed matter systems. *Wiley Interdiscip. Rev. Comput. Mol. Sci.* **4**, 15–25 (2014).
54. VandeVondele, J. et al. Quickstep: Fast and accurate density functional calculations using a mixed Gaussian and plane waves approach. *Comput. Phys. Commun.* **167**, 103–128 (2005).

Author contributions

I.Y. and J.Ga. conceived, coordinated the research and designed the experiments in close collaboration with V.V.S. I.Y. synthesized and characterized most catalysts and performed all catalytic tests with support from M.R. and I.V.S.M. and J.P.R. provided several demetallated zeolite catalysts and J.S.M.E. and M.M. provided the ZSM-5 nanosheets and performed the methylation reactions. S.B., K.D.W. and V.V.S. performed the DFT and ab initio MD calculations. B.M. and E.A.H. performed NMR characterization and J.Go. performed the in situ UV–vis analysis. All authors contributed to analysis and discussion of the data. The manuscript was primarily written by I.Y., K.D.W., V.V.S and J.Ga. with input from all authors.

Competing interests

The authors declare no competing interests.

Additional information

Supplementary information is available for this paper at https://doi.org/10.1038/s41557-018-0081-0.

Reprints and permissions information is available at www.nature.com/reprints.

Correspondence and requests for materials should be addressed to J.G.

Publisher's note: Springer Nature remains neutral with regard to jurisdictional claims in published maps and institutional affiliations.